LETTER

https://doi.org/10.1038/s41586-018-0856-x

Structure of the post-translational protein translocation machinery of the ER membrane

Xudong Wu[1,2], Cerrone Cabanos[1,2] & Tom A. Rapoport[1,2]*

Many proteins must translocate through the protein-conducting Sec61 channel in the eukaryotic endoplasmic reticulum membrane or the SecY channel in the prokaryotic plasma membrane[1,2]. Proteins with highly hydrophobic signal sequences are first recognized by the signal recognition particle (SRP)[3,4] and then moved co-translationally through the Sec61 or SecY channel by the associated translating ribosome. Substrates with less hydrophobic signal sequences bypass the SRP and are moved through the channel post-translationally[5,6]. In eukaryotic cells, post-translational translocation is mediated by the association of the Sec61 channel with another membrane protein complex, the Sec62–Sec63 complex[7–9], and substrates are moved through the channel by the luminal BiP ATPase[9]. How the Sec62–Sec63 complex activates the Sec61 channel for post-translational translocation is not known. Here we report the electron cryo-microscopy structure of the Sec complex from *Saccharomyces cerevisiae*, consisting of the Sec61 channel and the Sec62, Sec63, Sec71 and Sec72 proteins. Sec63 causes wide opening of the lateral gate of the Sec61 channel, priming it for the passage of low-hydrophobicity signal sequences into the lipid phase, without displacing the channel's plug domain. Lateral channel opening is triggered by Sec63 interacting both with cytosolic loops in the C-terminal half of Sec61 and transmembrane segments in the N-terminal half of the Sec61 channel. The cytosolic Brl domain of Sec63 blocks ribosome binding to the channel and recruits Sec71 and Sec72, positioning them for the capture of polypeptides associated with cytosolic Hsp70[10]. Our structure shows how the Sec61 channel is activated for post-translational protein translocation.

The Sec61 channel is formed from the multiple-membrane-spanning Sec61 protein and two single-membrane-spanning proteins (Sbh1 and Sss1 in *S. cerevisiae*)[7,8]. Sec61 and its prokaryotic homologue SecY consist of two halves that form an hourglass-shaped pore with a constriction in the middle of the membrane, a plug domain in the luminal or extracellular cavity, and a lateral gate, which opens to the surrounding lipid phase[11–16]. The idle, closed Sec61 channel is first primed for protein translocation by the binding of a channel partner, the ribosome or the Sec62–Sec63 complex[1,2]. Then, the translocating polypeptide inserts as a loop into the channel, with the hydrophobic part of the signal sequence moving through the lateral gate into the lipid phase, and the following segment of the polypeptide chain remaining in the channel pore[13,16].

In *S. cerevisiae*, the Sec complex contains the trimeric Sec61 complex and the tetrameric Sec62–Sec63 complex, consisting of Sec62, Sec63, Sec71 (also known as Sec66), and Sec72[7,8]. Sec62 and Sec63 are essential for cell viability and are predicted to have two and three transmembrane segments, respectively[17,18]. Sec63 contains a luminal J domain, which activates the BiP ATPase to bind to the incoming substrate, preventing it from sliding back to the cytosol[9]. Sec71 and Sec72 are not essential[19] and do not exist in higher organisms. Sec71 is a

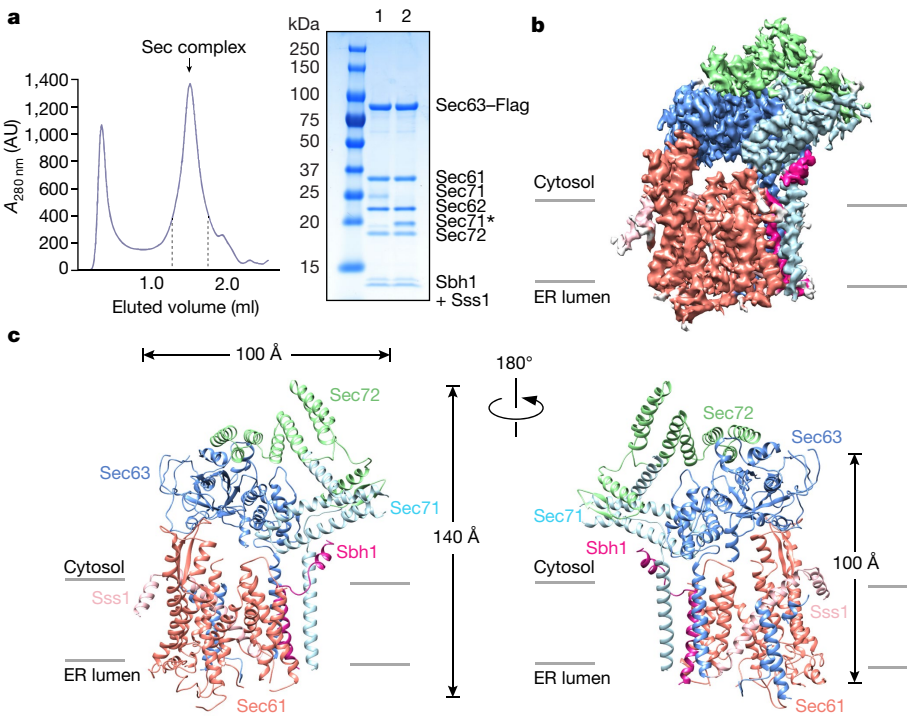

Fig. 1 | Overall structure of the Sec complex. **a**, The Sec complex was purified by using a Flag tag on Sec63, followed by gel filtration (left). The indicated fractions were combined and analysed by SDS–PAGE and Coomassie blue staining (lane 1). Endoglycosidase H treatment (lane 2) cleaves the glycan from Sec71 (resulting in the Sec71* band). AU, arbitrary units. The experiment was repeated independently five times. **b**, Side view of the density map with regions of the Sec complex components shown as different colours. The map is shown at contour level 0.028, with the exception of the Sec71 portion, which is shown at contour level 0.02. **c**, Side views of the models of the Sec complex components in a ribbon diagram.

[1]Howard Hughes Medical Institute, Harvard Medical School, Boston, MA, USA. [2]Department of Cell Biology, Harvard Medical School, Boston, MA, USA. *e-mail: tom_rapoport@hms.harvard.edu

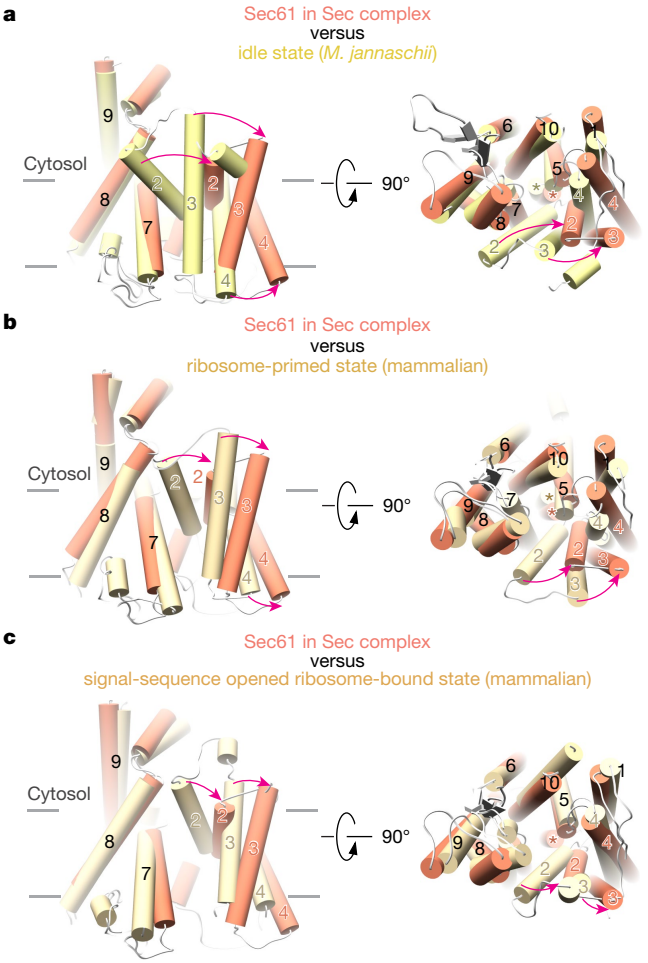

Fig. 2 | Lateral gate changes of the Sec61 channel in the Sec complex. **a**, The structure of Sec61 in the Sec complex is superimposed on that of the idle channel from *M. jannaschii* (PDB code 1RH5). Shown are the transmembrane segments as cylinders, viewed from the side (left) and from the cytosol (right). Movements of transmembrane segments are indicated by red arrows. The plug domains are indicated by asterisks in the right panel. **b**, As in **a**, but comparison is with the ribosome-primed Sec61 complex (PDB code 3J7Q). **c**, As in **a**, but comparison is with the ribosome-bound Sec61 channel (PDB code 3JC2) opened by a signal sequence.

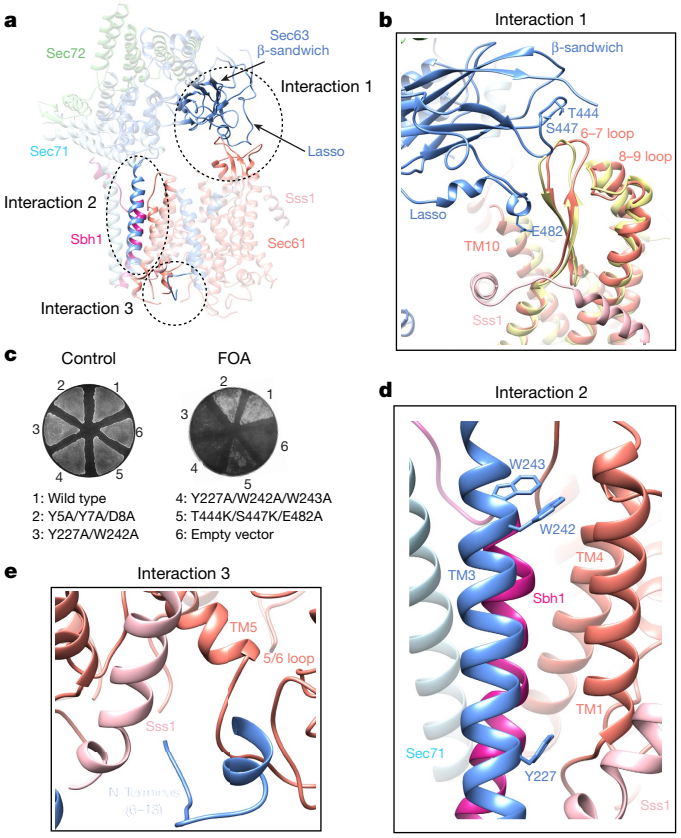

Fig. 3 | Interactions of Sec63 with the Sec61 channel. **a**, The interaction sites are indicated by dashed ovals and numbered. **b**, Magnified view of interaction 1. The Brl domain of Sec63 binds through the tip of a β-sandwich and a lasso loop to the TM6–TM7 and TM8–TM9 loops of Sec61. Mutated conserved Sec63 residues at the interfaces are shown as sticks. For comparison, the same Sec61 region is also shown for the ribosome-bound channel (yellow). **c**, Wild-type Sec63 was expressed from a URA plasmid in Sec63-lacking *S. cerevisiae* cells, together with wild-type or mutant Sec63. The cells were plated on 5-fluoroorotic acid (FOA) to select for cells that have lost the URA plasmid. Control experiments were carried out on medium without FOA. The sections on the plate are numbered as follows: (1) wild-type Sec63; (2) mutations in interface 3; (3) and (4) mutations in interface 2; (5) mutations in interface 1; (6) empty vector. The experiment was independently repeated twice. **d**, Magnified view of interaction 2. TM3 of Sec63 interacts with TM1 of Sec61 and the transmembrane segments of Sbh1 and Sss1. Trp and Tyr residues involved in the interaction are shown as sticks. **e**, Magnified view of interaction 3. The N terminus of Sec63 wedges between Sss1 and the TM5–TM6 loop of Sec61.

single-membrane-spanning protein that anchors the Hsp70-interacting Sec72 protein to the endoplasmic reticulum membrane[20]. In humans, Sec62 and Sec63 are frequently mutated or overexpressed in various cancers and mutations in Sec63 can cause polycystic kidney disease[21].

For structure determination, the Sec complex was purified in digitonin via the Flag-tagged Sec63 subunit, followed by gel filtration (Fig. 1a). The purified complex contained all seven components: the Sec61 channel (Sec61, Sbh1 and Sss1) and the Sec62, Sec63, Sec71 and Sec72 proteins in approximately stoichiometric amounts (Fig. 1a). The purified Sec complex was analysed by single-particle electron cryo-microscopy (cryo-EM). To reduce particle aggregation and preferred orientation on the grids, the complex was modified at surface-exposed lysines with low-molecular-mass polyethylene glycol (PEG).

Following initial 2D classification, 3D classification and refinement of the cryo-EM particle images yielded a final electron-density map at an overall resolution of 4.1 Å (Fig. 1b; Extended Data Fig. 1; Extended Data Table 1). Atomic models were built into the map for Sec61, Sbh1, Sss1, Sec63 and most parts of Sec71 and Sec72 (Fig. 1c; examples of the fit into the map are shown in Extended Data Fig. 2). The luminal J domain of Sec63 is invisible and is therefore likely to be flexible. Density for Sec62 was weak, but was sufficient to dock a homology model of its cytosolic DEP-like domain (Extended Data Fig. 3a) and to identify of one of its transmembrane segments (Extended Data Fig. 3b).

In the structure of the Sec complex, the Sec61 channel undergoes major conformational changes compared to its idle state, exemplified by a structure of the SecY channel from *Methanococcus jannaschii*[11] (Fig. 2a). In the idle state, the channel is closed at its lateral gate, formed between transmembrane segment 7 (TM7) and TM8 on one side and TM2 and TM3 on the other. By contrast, in the Sec complex, the lateral gate is wide open. Lateral gate opening is caused by TM2 and TM3 moving outwards and by TM4 tilting on the luminal side (Fig. 2a). The remaining transmembrane segments undergo little change. As in the idle state, the plug domain of Sec61 is located at the centre of the channel (Fig. 2a; right), preventing ions and other small molecules from permeating (Extended Data Fig. 4). Thus, opening of the channel laterally and across the membrane are distinct events, with the latter requiring the insertion of a translocating polypeptide and displacement of the plug.

The binding of the Sec62–Sec63 complex to the Sec61 channel causes wide opening of the lateral gate. Ribosome binding opens the lateral gate to a lesser extent (Fig. 2b; Extended Data Fig. 5a), and even after insertion of a nascent chain, the ribosome-associated Sec61 channel

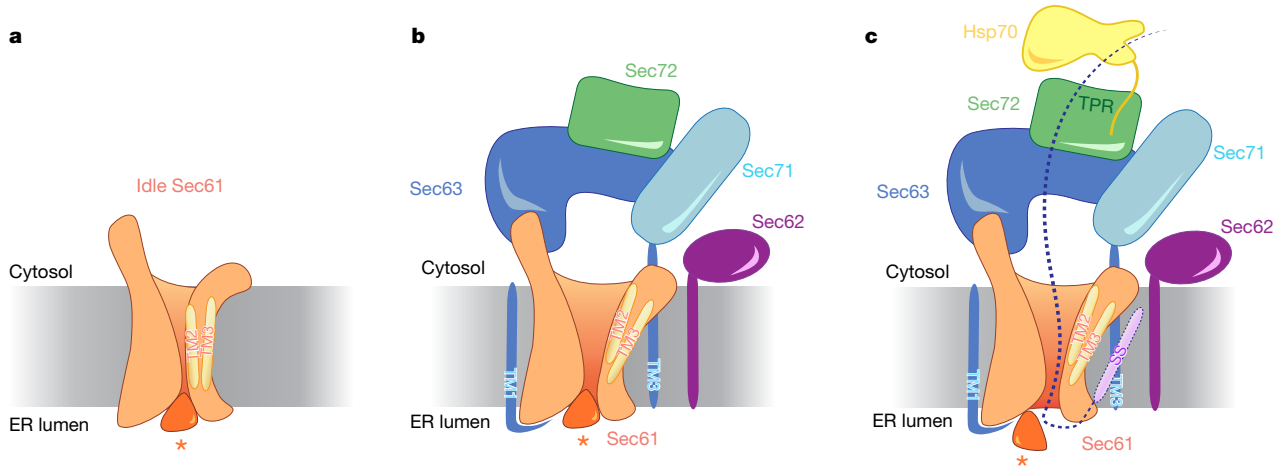

Fig. 4 | Scheme for insertion of a post-translational substrate into the Sec complex. a, Scheme of the idle Sec61 channel. The lateral and luminal gates are closed. The plug domain is indicated by a star. **b**, Scheme of the Sec62–Sec63-primed channel. The lateral gate is opened, caused by Sec63 serving as a scaffold. The channel is closed across the membrane by the plug. **c**, A post-translational substrate binds to Sec72 through associated Hsp70; the C terminus of Hsp70 binds to the TPR domain of Sec72. The polypeptide inserts as a loop into the Sec61 channel, with the signal sequence (SS) exiting the open lateral gate and binding to a groove on the outside. The plug is displaced. A transmembrane segment of Sec62 might stabilize the inserted signal sequence.

is not as open as the Sec61 channel in complex with Sec62–Sec63[16] (Fig. 2c). The width of the gate in the Sec complex even exceeds the width of the gate in a crystal structure of the *Pyrococcus furiosus* SecY channel in which opening was caused artificially by interaction with a neighbouring SecY molecule[14] (Extended Data Fig. 5b).

In the ribosome-primed state of the Sec61 channel, the lateral gate is only slightly open compared to the idle state (Extended Data Fig. 5a), such that the opening must widen substantially by thermal fluctuation to allow signal sequences to exit the channel into the lipid phase. This gate-opening energy must be compensated by energy gained from partitioning of a hydrophobic signal sequence into the hydrophobic lipid phase. In the post-translational Sec complex, the lateral channel gate does not require further opening to allow an α-helical signal sequence to exit into the lipid phase (Extended Data Fig. 5c). Thus, low-hydrophobicity signal sequences, which gain less free energy from lipid partitioning, can still function in post-translational translocation. In agreement with this model, mutations in a polar cluster at the lateral gate permit translocation of low-hydrophobicity signal sequences[22], most probably by favouring the open-gate conformation. In bacteria, the association of the SecA ATPase with the SecY channel, which primes the channel for post-translational translocation, also opens the lateral gate markedly more than ribosome binding, although in this case, TM7 and TM8 move, while the transmembrane segments of the N-terminal half of the channel remain unchanged[12,13]. Thus, the lateral gates are generally more open in Sec61 or SecY channels primed for post-translational translocation, thereby enabling function of signal sequences with lower hydrophobicity.

Opening of the lateral channel gate in the Sec complex is caused by Sec63. As predicted[18,23], Sec63 has three transmembrane segments and a large cytosolic Brl domain. The Brl domain of Sec63 binds to cytosolic loops TM6–TM7 and TM8–TM9 of Sec61 (Fig. 3a, interaction 1). Several conserved amino acid residues in the β-sandwich and lasso segments of the Brl domain face these loops, and the simultaneous mutation of these residues causes a strong defect in Sec63 function, as shown by compromised cell growth (Fig. 3b, c; sequence alignment and immunoblots for Sec63 expression are shown in Extended Data Figs. 6 and 7, respectively). A second interaction site is formed by TM3 of Sec63 binding to the other side of the channel, between TM1 of Sec61 and the transmembrane segments of Sbh1 and Sss1 (Fig. 3a, interaction 2, and Fig. 3d). Several conserved aromatic residues of TM3 (Trp242, Trp243 and Tyr227) are involved in the interaction with TM1 of Sec61; mutating these residues drastically reduces Sec63 function (Fig. 3c). Finally, the N terminus of Sec63 wedges on the luminal side of the channel between the TM5–TM6 loop and Sss1 (Fig. 3a, interaction 3, and Fig. 3e). This interface may be less important, as mutations in the N terminus of Sec63 do not affect its function (Fig. 3c). Because the conformations of loops TM6–TM7 and TM8–TM9 of Sec61 are essentially the same in the ribosome-bound and Sec62–Sec63-bound channels (Fig. 3b), interaction 1 with the C-terminal half of Sec61 can be considered a static anchor point for Sec63. The lateral gate is pried open by the additional interaction of Sec63 with the N-terminal half of Sec61 (interaction 2). Thus, Sec63 serves as a scaffold that imposes on Sec61 a gate-opened conformation. Since interactions 1 and 2 of Sec63 are required both for gate opening and cell viability (Fig. 3c), it is unlikely that the wide-open lateral gate is an artefact of sample preparation.

Sec63 not only activates the Sec61 channel for post-translational translocation, but its Brl domain also obstructs ribosome binding to Sec61 (Fig. 1c). A nascent polypeptide chain therefore cannot be transferred directly from the translating ribosome into the Sec61 channel. However, many proteins with low-hydrophobicity signal sequences begin their translocation through the Sec complex while the ribosome is still synthesizing the C-terminal part of the polypeptide chain[24,25]. The existence of free pools of Sec61 and Sec62–Sec63 sub-complexes in the endoplasmic reticulum[8] suggests that the Sec complex can dissociate, enabling the Sec61 channel to switch between the ribosome and Sec62–Sec63 partners.

The Sec71–Sec72 sub-complex[20] rests on top of the Brl domain of Sec63 and engages in multiple interactions with Sec complex components (Fig. 1c). Sec62 binds through its cytosolic DEP domain to the acidic C terminus of Sec63 (Extended Data Fig. 3a), consistent with previous findings[26], but the role of the DEP domain remains unclear, as it is dispensable[26]. The hydrophobic part of a channel-inserted signal sequence can be photochemically cross-linked simultaneously to the lateral gate of Sec61 and either Sec62 or Sec71, which could not be distinguished in SDS–PAGE because of their similar size[27]. The present structure shows that the transmembrane segment of Sec71 is far away from the lateral gate, whereas a transmembrane segment of Sec62 is close to it (Extended Data Fig. 3b) and therefore likely to be the cross-linking partner. This transmembrane segment may therefore interact with a signal sequence within the membrane and facilitate its insertion.

The structure leads to a model for post-translational protein translocation (Fig. 4). First, the Sec62–Sec63 complex binds to the channel,

priming it for translocation. Sec63 opens the lateral gate by serving as a scaffold for the Sec61 channel. When a post-translational polypeptide substrate arrives, it is initially associated with cytosolic chaperones[28], including Hsp70, which cycle on and off. Then, the acidic C-terminal tail of Hsp70 (Ssa1–Ssa4 in *S. cerevisiae*) binds to the TPR domain of Sec72[20], positioning the bound substrate for subsequent transfer into the membrane channel. In higher organisms lacking Sec71 and Sec72, substrates might be targeted by calmodulin[29]. Next, the signal sequence moves through the lateral gate and docks into a groove on its outside[13,16], while the following polypeptide segment is located in the actual pore. At this point, the polypeptide can no longer be associated with chaperones, as there is not enough space for them between the Brl domain of Sec63 and the Sec61 channel (Fig. 1c). The chaperone-stripped region of the polypeptide chain must comprise at least 40 residues following the signal sequence, as the distance from the top of the Brl domain to the luminal end of the Sec61 channel is ~100 Å (Fig. 1c). Indeed, all chaperones dissociate upon substrate insertion into the Sec complex[28]. The structure of the Sec complex explains why post-translational substrates are either short and devoid of bound chaperones[29,30], or loosely folded polypeptides associated with Hsp70[10,28].

Online content

Any methods, additional references, Nature Research reporting summaries, source data, statements of data availability and associated accession codes are available at https://doi.org/10.1038/s41586-018-0856-x.

Received: 25 November 2018; Accepted: 18 December 2018;
Published online 31 December 2018.

1. Voorhees, R. M. & Hegde, R. S. Toward a structural understanding of co-translational protein translocation. *Curr. Opin. Cell Biol.* **41**, 91–99 (2016).
2. Rapoport, T. A., Li, L. & Park, E. Structural and mechanistic insights into protein translocation. *Annu. Rev. Cell Dev. Biol.* **33**, 369–390 (2017).
3. Saraogi, I. & Shan, S.-O. Co-translational protein targeting to the bacterial membrane. *Biochim. Biophys. Acta* **1843**, 1433–1441 (2014).
4. Wild, K., Halic, M., Sinning, I. & Beckmann, R. SRP meets the ribosome. *Nat. Struct. Mol. Biol.* **11**, 1049–1053 (2004).
5. Ng, D. T., Brown, J. D. & Walter, P. Signal sequences specify the targeting route to the endoplasmic reticulum membrane. *J. Cell Biol.* **134**, 269–278 (1996).
6. Ast, T., Cohen, G. & Schuldiner, M. A network of cytosolic factors targets SRP-independent proteins to the endoplasmic reticulum. *Cell* **152**, 1134–1145 (2013).
7. Deshaies, R. J., Sanders, S. L., Feldheim, D. A. & Schekman, R. Assembly of yeast Sec proteins involved in translocation into the endoplasmic reticulum into a membrane-bound multisubunit complex. *Nature* **349**, 806–808 (1991).
8. Panzner, S., Dreier, L., Hartmann, E., Kostka, S. & Rapoport, T. A. Posttranslational protein transport in yeast reconstituted with a purified complex of Sec proteins and Kar2p. *Cell* **81**, 561–570 (1995).
9. Matlack, K. E., Misselwitz, B., Plath, K. & Rapoport, T. A. BiP acts as a molecular ratchet during posttranslational transport of prepro-α factor across the ER membrane. *Cell* **97**, 553–564 (1999).
10. Deshaies, R. J., Koch, B. D., Werner, W. M., Craig, E. A. & Schekman, R. A subfamily of stress proteins facilitates translocation of secretory and mitochondrial precursor polypeptides. *Nature* **332**, 800–805 (1988).
11. van den Berg, B. et al. X-ray structure of a protein-conducting channel. *Nature* **427**, 36–44 (2004).
12. Zimmer, J., Nam, Y. & Rapoport, T. A. Structure of a complex of the ATPase SecA and the protein-translocation channel. *Nature* **455**, 936–943 (2008).
13. Li, L. et al. Crystal structure of a substrate-engaged SecY protein-translocation channel. *Nature* **531**, 395–399 (2016).
14. Egea, P. F. & Stroud, R. M. Lateral opening of a translocon upon entry of protein suggests the mechanism of insertion into membranes. *Proc. Natl Acad. Sci. USA* **107**, 17182–17187 (2010).
15. Voorhees, R. M., Fernandez, I. S., Scheres, S. H. & Hegde, R. S. Structure of the mammalian ribosome–Sec61 complex to 3.4 Å resolution. *Cell* **157**, 1632–1643 (2014).
16. Voorhees, R. M. & Hegde, R. S. Structure of the Sec61 channel opened by a signal sequence. *Science* **351**, 88–91 (2016).
17. Deshaies, R. J. & Schekman, R. Structural and functional dissection of Sec62P, a membrane-bound component of the yeast endoplasmic reticulum protein import machinery. *Mol. Cell. Biol.* **10**, 6024–6035 (1990).
18. Feldheim, D., Rothblatt, J. & Schekman, R. Topology and functional domains of Sec63p, an endoplasmic reticulum membrane protein required for secretory protein translocation. *Mol. Cell. Biol.* **12**, 3288–3296 (1992).
19. Feldheim, D., Yoshimura, K., Admon, A. & Schekman, R. Structural and functional characterization of Sec66p—a new subunit of the polypeptide translocation apparatus in the yeast endoplasmic reticulum. *Mol. Biol. Cell* **4**, 931–939 (1993).
20. Tripathi, A., Mandon, E. C., Gilmore, R. & Rapoport, T. A. Two alternative binding mechanisms connect the protein translocation Sec71/Sec72 complex with heat shock proteins. *J. Biol. Chem.* **292**, 8007–8018 (2017).
21. Linxweiler, M., Schick, B. & Zimmermann, R. Let's talk about Secs: Sec61, Sec62 and Sec63 in signal transduction, oncology and personalized medicine. *Signal Transduct. Target. Ther.* **2**, 17002 (2017).
22. Trueman, S. F., Mandon, E. C. & Gilmore, R. A gating motif in the translocation channel sets the hydrophobicity threshold for signal sequence function. *J. Cell Biol.* **199**, 907–918 (2012).
23. Ponting, C. P. Proteins of the endoplasmic-reticulum-associated degradation pathway: domain detection and function prediction. *Biochem. J.* **351**, 527–535 (2000).
24. Jan, C. H., Williams, C. C. & Weissman, J. S. Principles of ER cotranslational translocation revealed by proximity-specific ribosome profiling. *Science* **346**, 1257521 (2014).
25. Costa, E. A., Subramanian, K., Nunnari, J. & Weissman, J. S. Defining the physiological role of SRP in protein-targeting efficiency and specificity. *Science* **359**, 689–692 (2018).
26. Wittke, S., Dünnwald, M. & Johnsson, N. Sec62p, a component of the endoplasmic reticulum protein translocation machinery, contains multiple binding sites for the Sec-complex. *Mol. Biol. Cell* **11**, 3859–3871 (2000).
27. Plath, K., Wilkinson, B. M., Stirling, C. J. & Rapoport, T. A. Interactions between Sec complex and prepro-α-factor during posttranslational protein transport into the endoplasmic reticulum. *Mol. Biol. Cell* **15**, 1–10 (2004).
28. Plath, K. & Rapoport, T. A. Spontaneous release of cytosolic proteins from posttranslational substrates before their transport into the endoplasmic reticulum. *J. Cell Biol.* **151**, 167–178 (2000).
29. Shao, S. & Hegde, R. S. A calmodulin-dependent translocation pathway for small secretory proteins. *Cell* **147**, 1576–1588 (2011).
30. Müller, G. & Zimmermann, R. Import of honeybee prepromelittin into the endoplasmic reticulum: energy requirements for membrane insertion. *EMBO J.* **7**, 639–648 (1988).

Acknowledgements We thank Z. Yu, R. Huang, and H.-T. Chou at the HHMI Janelia Cryo-EM Facility for help with microscope operation and data collection, E. Twomey for help with data analysis, R. Gilmore for advice and materials, and S. Shao and M. Catipovic for comments on the manuscript. This work was supported by a Jane Coffin Child fellowship to X.W., and an NIGMS award (R01GM052586) to T.A.R. T.A.R. is a Howard Hughes Medical Institute Investigator.

Reviewer information *Nature* thanks G. von Heijne and the other anonymous reviewer(s) for their contribution to the peer review of this work.

Author contributions X.W. designed experiments, purified proteins, collected and analysed electron microscopy data, and built the models. C.C. purified proteins, performed mutagenesis and mutant analysis. T.A.R. supervised the project. T.A.R. and X.W. wrote the manuscript.

Competing interests The authors declare no competing interests.

Additional information
Extended data is available for this paper at https://doi.org/10.1038/s41586-018-0856-x.
Supplementary information is available for this paper at https://doi.org/10.1038/s41586-018-0856-x.
Reprints and permissions information is available at http://www.nature.com/reprints.
Correspondence and requests for materials should be addressed to T.A.R.
Publisher's note: Springer Nature remains neutral with regard to jurisdictional claims in published maps and institutional affiliations.

METHODS

No statistical methods were used to predetermine sample size. The experiments were not randomized and the investigators were not blinded to allocation during experiments and outcome assessment.

Yeast strains and plasmids. For purification of endogenous Sec complex, a Flag tag was inserted at the C terminus of Sec63 at its genomic locus in the wild-type *S. cerevisiae* strain BY4741. The strain used for FOA selection of Sec63 mutants was provided by R. Gilmore. The strain lacks the endogenous *SEC63*, *URA* and *LEU* genes and expresses instead wild-type Sec63 under its endogenous promoter from a plasmid containing the URA marker. This strain was transformed with pRS315 plasmids containing the Leu marker, which express wild-type or mutant Sec63, under the endogenous promoter, with a Flag tag at the C terminus.

Protein purification. The BY4741 strain with C-terminally Flag-tagged endogenous Sec63 was first grown in YPD containing 0.2 μg/ml geneticin in a shaker at 230 r.p.m. overnight at 30 °C. A large culture was inoculated by diluting the starter culture 1:80 into YPD containing 0.2 μg/ml geneticin and then incubated at 30 °C for 20 h. The cells were pelleted and frozen until use.

Purification of the Sec complex was carried out as follows. In brief, 100 g of cell pellet was resuspended in 150 ml buffer A (50 mM HEPES pH 7.4, 150 mM NaCl) supplemented with a home-made protease inhibitor cocktail. The cells were lysed in a BioSpec Beadbeater for 35 min with 20-s/60-s on/off cycles in a water-ice bath. After lysis, cell debris was pelleted by centrifugation at 8,000*g* for 10 min. The supernatant was subjected to centrifugation in a Ti45 rotor (Beckman) at 43,000 r.p.m. for 1 h at 4 °C. The pelleted membranes were resuspended with a Dounce homogenizer in buffer A and pelleted again by centrifugation. This washed membrane fraction was flash-frozen in liquid nitrogen and kept at −80 °C. For protein purification, the membranes were thawed and resuspended with a Dounce homogenizer and solubilized by stirring at 4 °C for 2 h in buffer B (50 mM HEPES pH 7.5, 0.4 M NaCl, 10% glycerol, 5 mM $MgCl_2$, 5 mM EDTA, 1% digitonin) and protease inhibitors. Insoluble material was then removed by centrifugation at 43,000 r.p.m. for 30 min. The supernatant was incubated with 1 ml anti-Flag M2 resin (Sigma) for 3 h. The beads were washed with 10 ml buffer C (50 mM HEPES pH 7.5, 0.4 M NaCl, 10% glycerol, 0.05% digitonin), and the complex was eluted with 4 ml buffer B containing 0.2 mg/ml 3× Flag peptide (Sigma). The complex was concentrated and further purified by size-exclusion chromatography on a Superose 6 3.2/300 Increase column, equilibrated with buffer D (25 mM HEPES pH 7.4, 150 mM NaCl, 0.05% digitonin). Peak fractions were pooled and concentrated to 6 mg/ml for cryo-EM analysis.

Cryo-EM sample preparation and data acquisition. The concentrated sample was incubated with $MS(PEG)_{12}$ methyl-PEG-NHS-ester (Thermo Fisher) at a 1:40 molar ratio for 2 h on ice to reduce preferred orientation of particles on the grids. The PEGylated sample was applied to a glow-discharged quantifoil grid (1.2/1.3, 400 mesh). The grids were blotted for 2.5 s at ~90% humidity and plunge-frozen in liquid ethane using a Cryoplunge 3 System (Gatan).

Cryo-EM data were collected on a Titan Krios electron microscope (FEI) operated at 300 kV and equipped with a K2 Summit direct electron detector (Gatan) at HHMI Janelia Farm. A Gatan Imaging filter with a slit width of 20 eV was used to remove inelastically scattered electrons. All cryo-EM movies were recorded in super-resolution counting mode using SerialEM. The nominal magnification of 81,000× corresponds to a calibrated physical pixel size of 1.35 Å and 0.675 Å in the super-resolution mode. The dose rate was 5.48 electrons $Å^{-2}$ s^{-1}. The total exposure time was 10 s, resulting a total dose of 54.8 electrons $Å^{-2}$ fractionated into 50 frames (200 ms per frame). The defocus range for the sample was between 1.0 and 2.8 μm.

Image processing. A total of 7,504 dose-fractionated super-resolution movies were subjected to motion correction using the program MotionCor2[31] with 2× binning, yielding a pixel size of 1.35 Å. A sum of all frames of each image stack (50 in total) was calculated following a dose-weighting scheme and used for all image-processing steps except for defocus determination. The program Gctf[32] was used to estimate defocus values of the summed images from all movie frames without dose weighting. Particles were autopicked by Gautomatch (http://www.mrc-lmb.cam.ac.uk/kzhang/). After manual inspection and sorting to discard poor images, classifications were done in Relion 3.0[33]. A total of 2,280,162 particles was extracted and subjected to one round of reference-free 2D classification to remove false picks and obvious junk classes. To speed up 3D classification during data collection, data were analysed in 4 batches in the order of their collection, and each batch was subjected to 3D classification, using as reference an initial model obtained from a previous small data set collected on a Talos microscope. Only one class, containing 727,077 particles, showed protein features and particles from this class were combined for further classification. Another round of global 3D classification with 6 classes was carried out and one class with the complete Sec complex and good secondary structure features was selected (322,182 particles). Auto-refinement was done on this particle set using the reconstruction from previous 3D classification as initial model and a soft mask surrounding the protein and detergent micelle. After this round of refinement, particles were subjected to Bayesian polishing, followed by another round of auto-refinement and focused refinement using a mask encompassing Sec61–Sec63–Sec71–Sec72. The refinement at this step yielded a 4.3 Å map. Using the angle assignments obtained after the focused refinement, a 1.8 degree local 3D classification (2 sigma and T20) with an adaptive mask for Sec61–Sec63–Sec71–Sec72 was used to further classify the particles. A total of 190,704 particles was selected and subjected to another round of auto-refinement. 3D classification (T30) without alignment, but with a mask, was used to further improve the quality of the map. After selection of 91,218 particles, a final round of auto-refinement followed by focused refinement using the adaptive mask yielded a map at 4.1 Å. Local resolution was calculated by Resmap[34] and map sharpening was performed in Relion 3.0. All reported resolutions are based on gold-standard refinement procedures and the FSC = 0.143 criterion. To generate a map filtered to local resolution, the map refined in Relion3.0 was imported into cryoSPARC2[35]. A *B*-factor of −180 was applied. All software is supported by SBGrid[36].

Model building. All model building was done in Coot. For building of the Sec63 model, three transmembrane helices could be easily identified and were initially built as poly-Ala. A homology model was generated for the large cytosolic Brl (Brr2-like) domain of Sec63 using RaptorX[37], on the basis of its similarity with domains found in RNA helicases, including the Brr2 protein involved in splicing[23]. The model was then docked into the density map, C_α-backbone atoms were adjusted, and the registry checked and modified, using secondary structure prediction and residues with bulky side-chains (Trp, Tyr, Phe, His and Arg) as guidance. For building of models for Sec61, Sss1 and Sbh1, homology models for each individual component were first generated with RaptorX. These models were modified as for Sec63. For Sec71 and Sec72, homology models were generated using RaptorX, based on previous crystal structures of a thermophilic species[20]. Atomic models were built for these proteins, except for Sec72 residues 1–100. The manually built models were then refined using Phenix[38]. For the figures, the Sec72 segment (residues 1–100) was included and docked as a rigid body into the map with slight modifications. A homology model of the DEP-like domain of Sec62, predicted by RaptorX[37] and other servers, was fit as a rigid body into the map.

Mutagenesis experiments. Constructs carrying wild-type Sec63 or mutants were transformed into the strain described above. Transformed yeast cells were plated on Leu/Ura double drop-out plates and allowed to grow for three days. Multiple colonies were mixed and streaked out again on Leu/Ura double drop-out plates. For each construct, the same number of cells were diluted in water and then grown on Leu drop-out plates containing FOA or on Leu/Ura double drop-out plates as a control. Plates were incubated at 30 °C for 2–3 days before imaging.

Reporting summary. Further information on research design is available in the Nature Research Reporting Summary linked to this paper.

Data availability

The coordinates of atomic models of the Sec complex without Sec62 were deposited in the Protein Data Bank with accession code 6ND1. The cryo-EM maps of the Sec complex before and after focused refinement with a mask were deposited with accession code EMDB-0440. All other data are available on reasonable request from the corresponding author.

31. Zheng, S., Palovcak, E., Armache, J.-P., Cheng, Y. & Agard, D. MotionCor2: anisotropic correction of beam-induced motion for improved cryo-electron microscopy. *Nat. Methods* **14**, 331–332 (2017).
32. Zhang, K. Gctf: real-time CTF determination and correction. *J. Struct. Biol.* **193**, 1–12 (2016).
33. Zivanov, J. et al. New tools for automated high-resolution cryo-EM structure determination in RELION-3. *eLife* **7**, e42166 (2018).
34. Kucukelbir, A., Sigworth, F. J. & Tagare, H. D. Quantifying the local resolution of cryo-EM density maps. *Nat. Methods* **11**, 63–65 (2014).
35. Punjani, A., Rubinstein, J. L., Fleet, D. J. & Brubaker, M. A. cryoSPARC: algorithms for rapid unsupervised cryo-EM structure determination. *Nat. Methods* **14**, 290–296 (2017).
36. Morin, A. et al. Collaboration gets the most out of software. *eLife* **2**, e01456 (2013).
37. Källberg, M. et al. Template-based protein structure modeling using the RaptorX web server. *Nat. Protocols* **7**, 1511–1522 (2012).
38. Adams, P. D. et al. PHENIX: a comprehensive Python-based system for macromolecular structure solution. *Acta Crystallogr. D* **66**, 213–221 (2010).

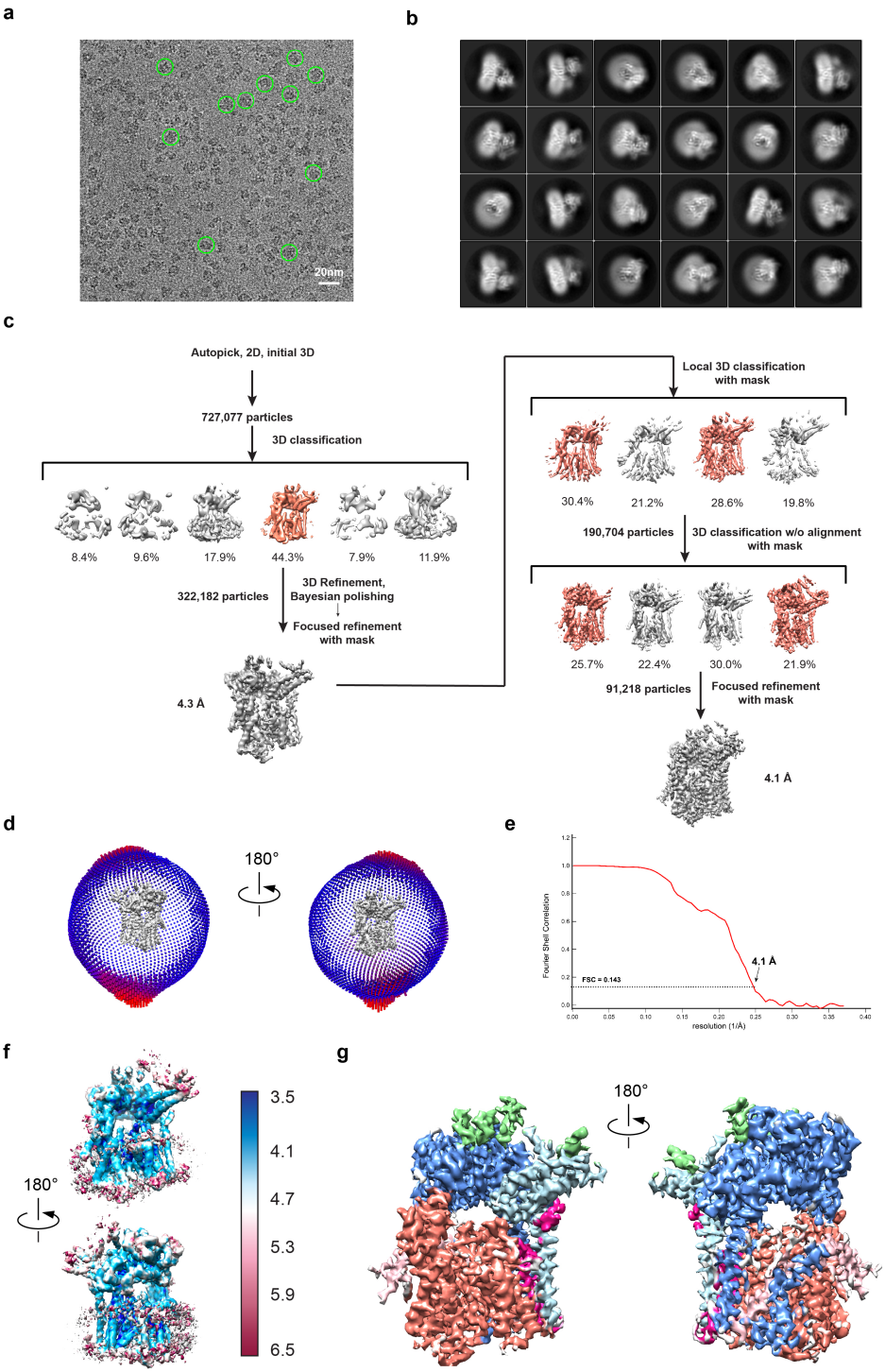

Extended Data Fig. 1 | Cryo-EM analysis of the Sec complex. a, The image shows a representative cryo-EM image of Sec-complex particles. Some particles are highlighted with green circles. Four electron microscopy grids were screened and had a similar particle distribution. **b**, Representative 2D class averages of picked particles collected from images of three grids. **c**, Image processing workflow for 3D classification and refinement. Shown are views of 3D reconstructions parallel to the membrane, with percentages of the particles in each class indicated. Classes in colour were used for subsequent analysis. **d**, Euler-angle distribution in two different views. **e**, Fourier shell correlation (FSC) curve with indicated resolution at FSC = 0.143. **f**, Local resolution was calculated from the unfiltered half-map and coloured according to the scale on the side. Two different views are shown. **g**, Map filtered to local resolution using cryoSPARC2. Regions corresponding to the different proteins are coloured as in Fig. 1b.

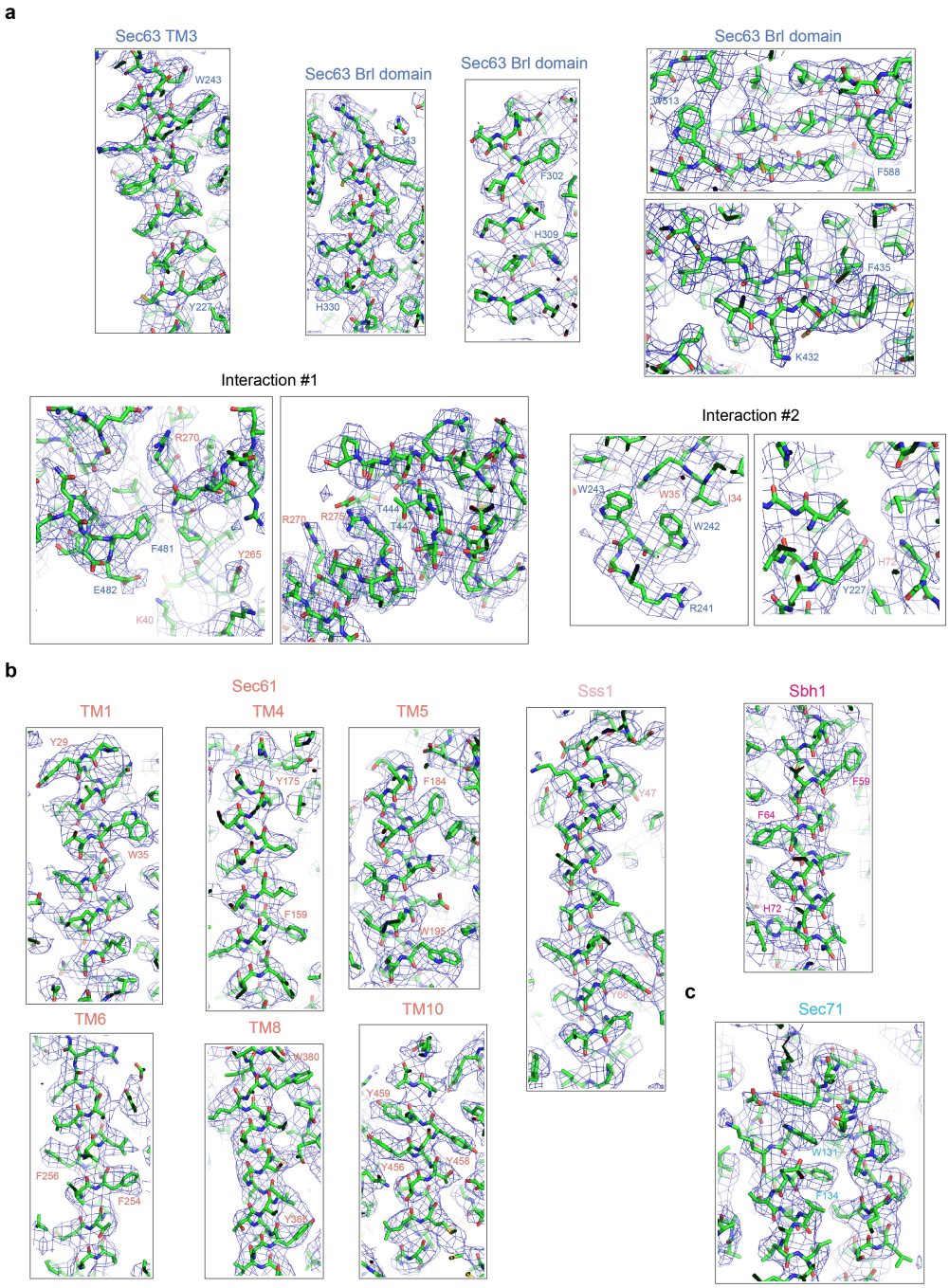

Extended Data Fig. 2 | Examples of the fit of the models into the density map. a, Density map and model for the indicated segments of Sec63. Interactions 1 and 2 show the interfaces between Sec63 and components of the Sec61 complex. Residues in salmon and pink belong to Sec61 and Sss1, respectively. **b**, As in **a**, but for segments of the Sec61 complex. **c**, As in **a**, but for the loop of Sec71 interacting with Sec63 and Sec61.

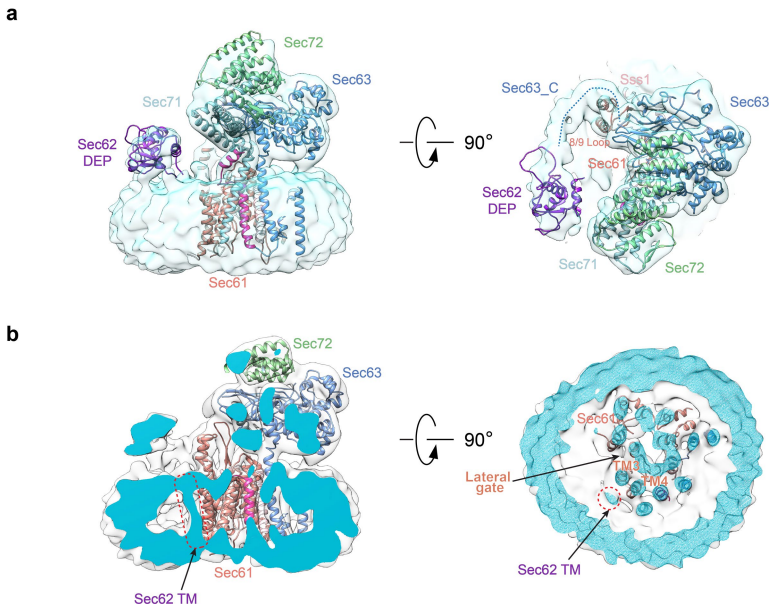

Extended Data Fig. 3 | Localization of Sec62 in the Sec complex. **a**, Shown is the unsharpened map (grey), low-pass filtered to 8 Å, with models for the components of the Sec complex in ribbon diagram. A homology model for the N-terminal DEP domain of Sec62 (purple) was docked into the map. The acidic C-terminal tail of Sec63 (dotted line on the right panel) wraps around the TM8–TM9 loop of Sec61 and interacts with the cytosolic DEP domain of Sec62. **b**, Cuts through the middle of the unsharpened map are shown in views from the side and from the cytosol. Density for a transmembrane segment of Sec62 (highlighted by red, dotted ovals) is close to the lateral gate.

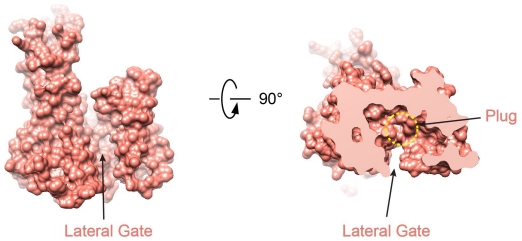

Extended Data Fig. 4 | The Sec61 channel in the Sec complex has open lateral and closed luminal gates. Space-filling model of the Sec61 channel in the Sec complex. The left panel shows a side view with the lateral gate in the front. The right panel shows a cut through the space-filling model viewed from the cytosol. Note that the plug domain keeps the luminal gate closed.

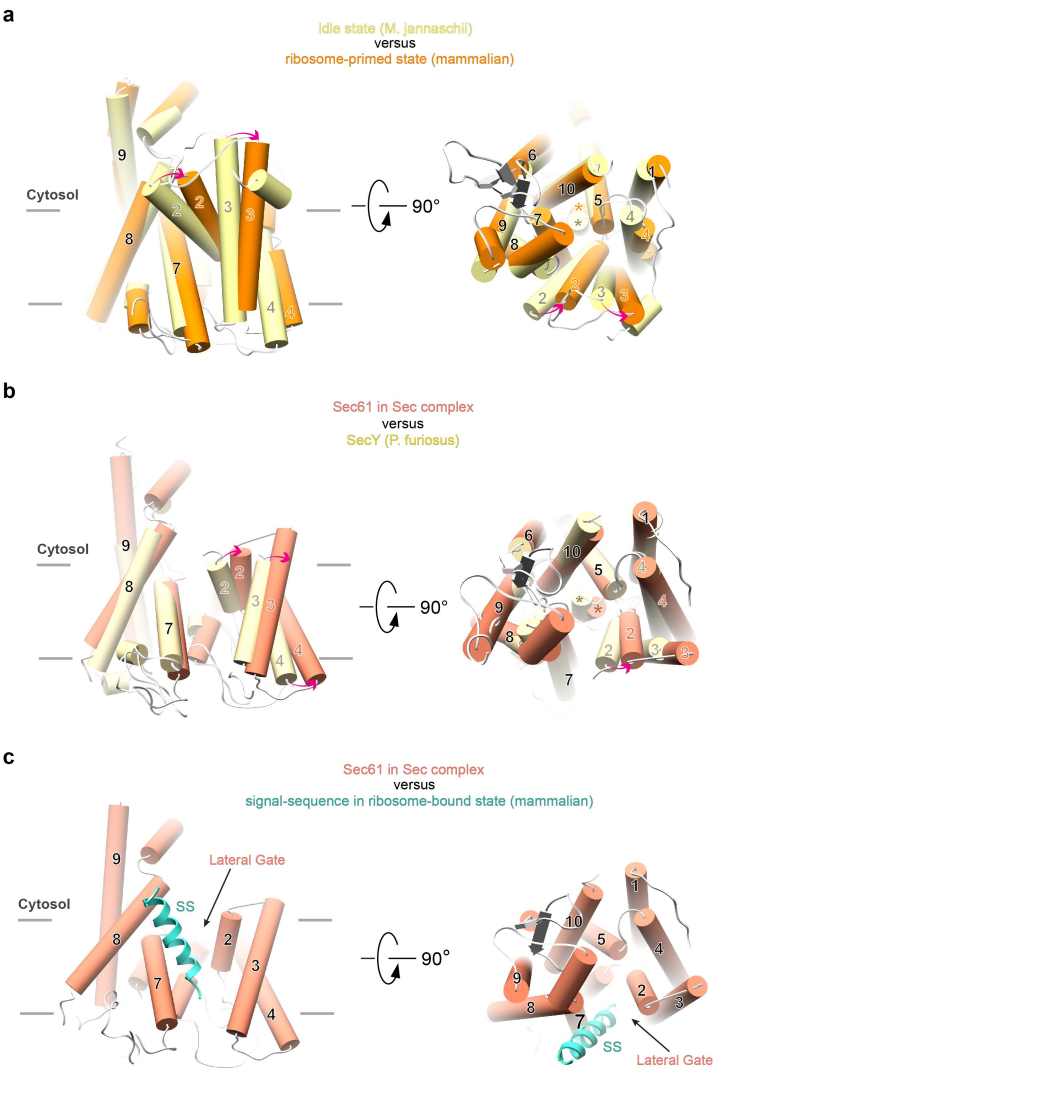

Extended Data Fig. 5 | Lateral gate changes of the Sec61 channel. **a**, The structure of Sec61 in the ribosome-primed state (PDB code 3J7Q) is superimposed on that of the idle channel from *M. jannaschii* (PDB code 1RH5). Shown are the transmembrane segments as cylinders, viewed from the side (left) and from the cytosol (right). Movements of transmembrane segments are indicated by red arrows. The plug domains are indicated by stars in the right panel. **b**, As in **a**, but comparison of the Sec61 channel in the Sec complex with the SecY channel from *P. furiosus* (PDB code 3MP7). **c**, The Sec61 channel in the Sec complex is shown together with the signal sequence (SS; in cyan) from a structure of the signal-sequence-opened ribosome-bound Sec61 channel (PDB code 3JC2). The alignment of the Sec61 molecules was done as in Fig. 2c. Note that the lateral gate in the Sec complex is open enough to allow a helix to move through.

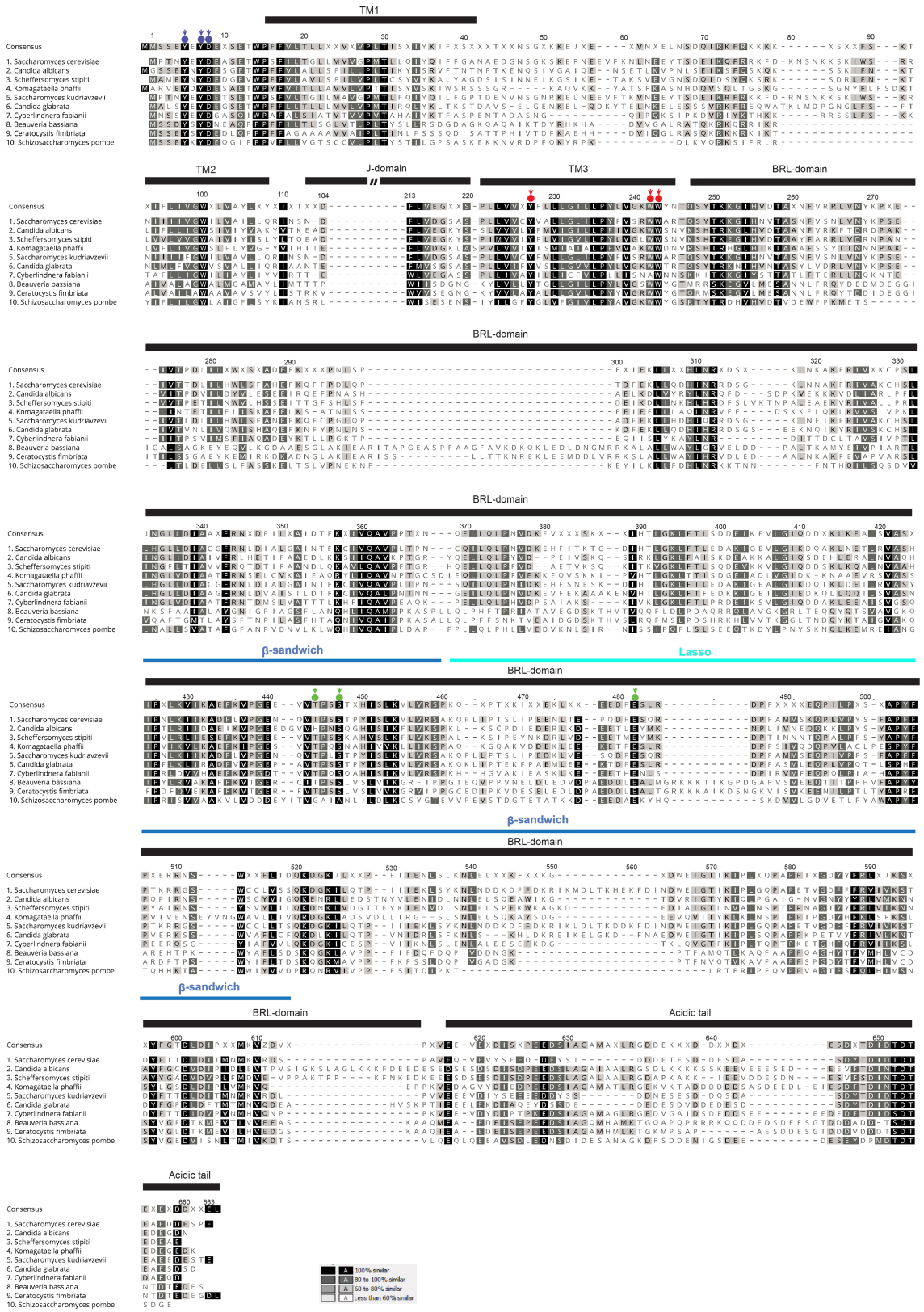

Extended Data Fig. 6 | Alignment of Sec63 sequences from different species. Transmembrane segments and the Brl and J domains are shown as black bars above the sequences. The β-sandwich and lasso regions in the Brl domain are indicated as blue lines. Conserved residues are highlighted. Mutated residues involved in the interaction with the Sec61 channel are shown as coloured circles and arrows: interaction 3 at the N terminus in blue; interaction 2 in TM3 in red; interaction 1 in the β-sandwich and lasso segments of the Brl domain in green.

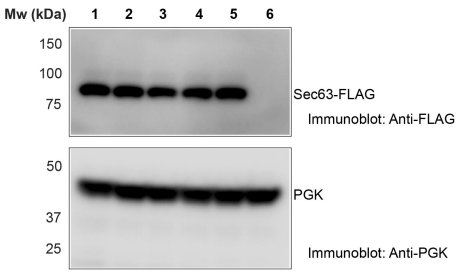

Extended Data Fig. 7 | Sec63 expression in wild-type and mutant *S. cerevisiae* cells. The strains used in Fig. 3c were analysed for expression of Flag-tagged Sec63. Flag-tagged wild-type or mutant Sec63 was expressed in *Sec63*Δ *S. cerevisiae* cells. Equal numbers of cells were analysed by SDS–PAGE, followed by immunoblotting with Flag antibodies. To control for equal loading, the samples were also analysed with antibodies to phosphoglycerate kinase (PGK). The lanes correspond to expression of the following Sec63 proteins: (1) wild-type Sec63; (2) mutations in interface 3 of Sec63 (Y5A/Y7A/D8A); (3) mutations in interface 2 (Y227A/W242A); (4) mutations in interface 2 (Y227A/W242A/W243A); (5) mutations in interface 1 (T444K/S447K/E482A); (6) empty vector. The experiment was repeated twice.

Extended Data Table 1 | Cryo-EM data collection, refinement, and validation statistics

	Sec Complex (EMDB-0440) (PDB 6ND1)
Data collection and processing	
Magnification	81,000
Voltage (kV)	300
Electron exposure (e–/Å^2)	54.8
Defocus range (μm)	-1.0 to -2.8
Pixel size (Å)	1.35
Symmetry imposed	C1
Initial particle images (no.)	2,280,162
Final particle images (no.)	91,218
Map resolution (Å)	4.1
FSC threshold	0.143
Map resolution range (Å)	3.5 to 6.5
Refinement	
Initial model used (PDB code)	
Model resolution (Å)	4.1
FSC threshold	0.5
Model resolution range (Å)	
Map sharpening *B* factor (Å^2)	-180
Model composition	
Non-hydrogen atoms	9189
Protein residues	1179
Ligands	
B factors (Å^2)	
Protein	72.61
Ligand	
R.m.s. deviations	
Bond lengths (Å)	0.009
Bond angles (°)	1.254
Validation	
MolProbity score	1.68
Clashscore	7.55
Poor rotamers (%)	0.1
Ramachandran plot	
Favored (%)	96.16
Allowed (%)	3.76
Disallowed (%)	0.08

nature research

Corresponding author(s): Tom Rapoport

Reporting Summary

Nature Research wishes to improve the reproducibility of the work that we publish. This form provides structure for consistency and transparency in reporting. For further information on Nature Research policies, see Authors & Referees and the Editorial Policy Checklist.

Statistical parameters

When statistical analyses are reported, confirm that the following items are present in the relevant location (e.g. figure legend, table legend, main text, or Methods section).

n/a	Confirmed
☐	☒ The exact sample size (*n*) for each experimental group/condition, given as a discrete number and unit of measurement
☐	☒ An indication of whether measurements were taken from distinct samples or whether the same sample was measured repeatedly
☒	☐ The statistical test(s) used AND whether they are one- or two-sided *Only common tests should be described solely by name; describe more complex techniques in the Methods section.*
☒	☐ A description of all covariates tested
☒	☐ A description of any assumptions or corrections, such as tests of normality and adjustment for multiple comparisons
☒	☐ A full description of the statistics including central tendency (e.g. means) or other basic estimates (e.g. regression coefficient) AND variation (e.g. standard deviation) or associated estimates of uncertainty (e.g. confidence intervals)
☒	☐ For null hypothesis testing, the test statistic (e.g. *F*, *t*, *r*) with confidence intervals, effect sizes, degrees of freedom and *P* value noted *Give P values as exact values whenever suitable.*
☒	☐ For Bayesian analysis, information on the choice of priors and Markov chain Monte Carlo settings
☒	☐ For hierarchical and complex designs, identification of the appropriate level for tests and full reporting of outcomes
☒	☐ Estimates of effect sizes (e.g. Cohen's *d*, Pearson's *r*), indicating how they were calculated
☒	☐ Clearly defined error bars *State explicitly what error bars represent (e.g. SD, SE, CI)*

Our web collection on statistics for biologists may be useful.

Software and code

Policy information about availability of computer code

Data collection	Serial EM
Data analysis	Gautomatch_v0.53, Gctf_v1.06, relion_3.0, resmap_v1.1.4

For manuscripts utilizing custom algorithms or software that are central to the research but not yet described in published literature, software must be made available to editors/reviewers upon request. We strongly encourage code deposition in a community repository (e.g. GitHub). See the Nature Research guidelines for submitting code & software for further information.

Data

Policy information about availability of data

All manuscripts must include a data availability statement. This statement should provide the following information, where applicable:

- Accession codes, unique identifiers, or web links for publicly available datasets
- A list of figures that have associated raw data
- A description of any restrictions on data availability

The coordinates of atomic models of the Sec complex without Sec62 were deposited in the Protein Data Bank with accession code 6ND1. The cryo-EM maps of the Sec complex before and after focused refinement with a mask were deposited with accession code EMD-0440. All other data are available on reasonable request from the corresponding authors.

Field-specific reporting

Please select the best fit for your research. If you are not sure, read the appropriate sections before making your selection.

☒ Life sciences ☐ Behavioural & social sciences ☐ Ecological, evolutionary & environmental sciences

For a reference copy of the document with all sections, see nature.com/authors/policies/ReportingSummary-flat.pdf

Life sciences study design

All studies must disclose on these points even when the disclosure is negative.

Sample size	The growth assay contains millions of cells and we are only looking for the growth of the population of a specific yeast strain.
Data exclusions	No data was excluded.
Replication	The results can be replicated.
Randomization	Randomization is unnecessary for structure work. For growth assay, all conditions including cell amount and temperature etc are kept as the same.
Blinding	Blinding is not performed, which is impossible for structure work.

Reporting for specific materials, systems and methods

Materials & experimental systems

n/a	Involved in the study
☒	☐ Unique biological materials
☐	☒ Antibodies
☒	☐ Eukaryotic cell lines
☒	☐ Palaeontology
☒	☐ Animals and other organisms
☒	☐ Human research participants

Methods

n/a	Involved in the study
☒	☐ ChIP-seq
☒	☐ Flow cytometry
☒	☐ MRI-based neuroimaging

Antibodies

Antibodies used	anti-FLAG antibody (M2, Sigma); anti-PGK antibody (22C5D8, Abcam)
Validation	All antibodies have been tested with positive controls with the specific epitopes.